Airborne Radar-Based Collision Detection and Risk Estimation for Small Unmanned Aircraft Systems

Laith R. Sahawneh[1], James Mackie[2], Jonathan Spencer[3], Randal W. Beard[4] and Karl F. Warnick[5]
Brigham Young University, Provo, Utah, 84602, USA

Airborne collision detection is a difficult problem due to inherent noise, errors in prediction and modeling the dynamics of intruder aircraft. Moreover, on-board limited computational resources, fast closing speeds and unanticipated maneuvers make it very challenging to detect collision without creating too many false alarms. In this paper, we present an innovative approach to quantify likely intruder trajectories and estimate the probability of collision risk for a pair of aircraft flying at the same altitude and in close proximity given the state estimates provided by an airborne radar sensor. The proposed approach is formulated in a probabilistic framework using the reachable set concept and the statistical data contained in the uncorrelated encounter model (UEM) developed by MIT Lincoln Laboratory. Monte Carlo based simulation is used to evaluate and compare the performance of the proposed approach with linear extrapolation collision detection logic.

---

[1] Research assistant, Department of Electrical and Computer Engineering, Brigham Young University, student member of AIAA.
[2] Research assistant, Department of Electrical and Computer Engineering, Brigham Young University.
[3] Research assistant, Department of Electrical and Computer Engineering, Brigham Young University.
[4] Professor, Department of Electrical and Computer Engineering, Brigham Young University, Associate Fellow of AIAA.
[5] Professor, Department of Electrical and Computer Engineering, Brigham Young University

I. Introduction

The potential of Unmanned Aircraft Systems (UAS) for commercial and civil use has been known for decades. Their use however has been limited by Federal Aviation Administration (FAA) regulations due to the risks they pose. Currently, unmanned aircraft systems face limitations on their access into the national airspace because they do not have the ability to sense and avoid other air traffic. Therefore, the need for a robust sense and avoid (SAA) system will be a crucial requirement for UAS to provide the equivalent level of safety (ELOS) as manned aircraft [1]. Small UAS are particularly attractive and their use is likely to grow more quickly in civil and commercial operations because of their versatility and relatively low initial cost and operating expenses.

A number of conflict and collision detection methods have been suggested in the context of air traffic management, mobile robotics and autonomous control. These different methods can be classified under four fundamental approaches: deterministic or straight line, worst case, probabilistic, and flight plan sharing [2–4]. Many of these methods stress the deterministic approach, where a single trajectory of the intruder is predicted using straight line extrapolation. This is a reasonable approach when there is a perfect knowledge of the states of the detected intruder. However in practice, the uncertainty free model could lead to erroneous prediction of collision threat particulary when solving the problem over a short time horizon. The term *"conflict"* is normally used in the context of manned aviation air traffic management and alerting systems. Conflict detection usually implies a multi-layer approach to detect loss of minimum separation, defined as an event where two or more aircraft come within 3-5 nautical miles over time horizons on the order of minutes [5, 6]. On the other hand, *"collision"* is used when detection is required for close proximity encounters over time horizons of seconds [4]. While, many of these techniques may apply for either conflict or collision detection, an appropriate scaling in design parameters, assumptions, and thresholds is required.

Less research has been dedicated to collision detection for UAS, mainly because this problem is relatively new in comparison with manned aviation air traffic management. Regardless, there is a growing body of research in sense and avoid for UAS, motivated by the need to integrate UAS into the national airspace, and in particular to establish separation standards, risk assessment, and collision

detection metrics [7–11]. The work by Temizer et al. proposed a comprehensive collision alerting and avoidance scheme for different sensor modalities, including radar. The problem is formulated as a Markov decision process (MDP) and a partially observable Markov decision process (POMDP) to account for sensors uncertainties. A generic MDP/POMDP solver can be used to generate avoidance strategies that optimize a cost function that includes minimizing probability of air collision event [9]. Our work is similar in providing analysis of multiple components of an aircraft alerting system, however we focus on the collision detection functionality. The current paper contributes to this body of work by introducing a feasible framework for sensing, tracking, and collision detection that can be integrated on-board small UAS. The primary focus of this paper is to develop an innovative approach to quantify likely intruder future trajectories and evaluate the collision risk for a pair of aircraft flying at the same altitude in close proximity. The proposed approach builds upon the reachability set concept and the statistical data contained in the uncorrelated encounter model (UEM) developed by MIT Lincoln Laboratory [12]. The main role of encounter models is to generate statistically representative traffic encounters to explore and evaluate the robustness and performance of a collision avoidance system. However, other ways to utilize these data sets have been suggested in the literature. For example, Jackson et al. used sampling methods to generate trajectories up to a future time of interest from MIT LL UEM data set to increase the fidelity of the reachability set boundary of the intruder [13]. Reachable sets of all possible positions of a moving object have been extensively studied, due to their importance in mobile robotics [14–17]. In this paper, we have obtained an analytical discrete-time approximation of the reachable sets over look-ahead time window using Dubins kinematic model of an aircraft flying at a constant altitude. Similar to Ref. [13], we have used reachable sets to predict the intruder's trajectory rather than predicting the ownship's ability to determine collision free space. Alternatively, rather than sampling, we infer a probability distribution from the transition probabilities contained in the MIT LL UEM and project it over a finite look-ahead time horizon. Then we assign these propagated probabilities to the discretized reachable sets that are used to compute collision risk.

Rather than simply adding artificial measurement noise, we incorporate in the analysis a realistic model for the radar sensor. While aspects of the work presented in section IV have appeared in [18],

this paper contains several distinct contributions. Namely, we have added a realistic sensor model along with an estimator whose process and measurement equations are formulated in the so-called modified polar coordinates (MPC) that appropriately handles polar measurements [19, 20]. Moreover, in this paper we analyze the radar sensor, the tracker and collision detection by comparing the proposed collision detection approach with a linear extrapolation method using simulated encounters generated from the MIT LL UEM. The performance is quantified in terms of the probability of detection and the probability of false alarm using Monte Carlo based simulations.

The rest of the paper is organized as follows. Section II gives a mathematical description of a Frequency Modulated Continuous Wave (FMCW) radar that is applicable for small UAS. An estimator to track current states of the detected intruder is presented in Section III. Section IV proposes a probabilistic framework for collision detection that quantifies likely intruder future trajectories. Section V derives a scheme to compute the probability risk of future collision events. Monte Carlo based simulation results obtained through comparing the performance of the proposed approach with linear extrapolation collision detection approach are reported in Section VI. Section VII concludes the paper.

II. Airborne Radar Sensor Model

In a sense and avoid system, the key factor in selecting a sensor is its ability to reliably measure range, bearing and elevation angles of the detected intruder. Using small UAS as a platform further restricts the size, weight, and power constraints (SWaP). Currently, electro-optical/infrared cameras, Radar, and Light Detection And Ranging (LIDAR) are examples of sensors used to detect non-cooperative traffic. Non-cooperative traffic means that no information about conflicting traffic is communicated or transmitted to the aircraft from the conflicting intruders or from Air Traffic Control (ATC). Alternatively, Traffic Collision Avoidance System (TCAS) and Automatic Dependent Surveillance-Broadcast (ADS-B) are two examples of systems for detecting cooperative intruders. Optical sensors, such as cameras are generally small and lightweight and offer excellent field of view and angle of arrival determination. IR cameras have the added advantage that they can be used at night [21]. However, both Optical and IR sensors are subject to signal degradation due

to weather, and both have difficulty determining range and velocity in high speed collision detection scenarios. Lidar is an extremely powerful imaging modality and is used extensively for mapping because it gives very precise range and angle measurements. Unfortunately, robust lidar systems are generally much too large to be integrated on small UAS and also suffer some of the same weather degradation as optical sensors [21].

Radar is an excellent choice for a sensor for an small UAS platform because of its capability to determine range and bearing to an intruder target in any weather condition. Because traditional pulsed radar systems are generally bulky and power hungry, we chose to model a Frequency Modulated Continuous Wave (FMCW) radar. Continuous wave radar systems such as FMCW radar use much lower levels of transmitted power making them optimal for small UAS applications. Although the processing for FMCW radar is more sophisticated than pulsed radar, advancements in computing have made these systems small enough to fit on small UAS platforms [22].

A limitation of radar is that the signal strength of the return is dependent on the material properties of the intruder aircraft, the frequency used, and the angle at which the aircraft is observed [21]. This is represented in a radar cross section (RCS) profile that is specific to each aircraft and varies as a function of angle. For the simulations we modeled three different sizes of aircraft by using three different values of RCS which are listed in Section IV. Although RCS can have variations in angle and time due to moving parts, the authors used constant values for simulated RCS. This approach is justified because of the temporal integration inherent in FMCW radar as well as significant averaging applied in post processing. Any small RCS variations in time will average to a relatively constant value. Thus, constant values are used for simulated RCS in order to simplify the model, yet maintain proof of concept.

Our model implements a monopulse configuration with a single transmit antenna and two receive antennas fixed on a rotating gimbal. All antennas are modeled with a sinc radiation pattern. The two receive antennas have a 3 dB beamwidth of 20 degrees and are offset ± 10 degrees from the transmit antenna. The transmit antenna has a 3 dB beamwidth of 40 degrees and is angled at the monopulse system boresight, or the gimbal angle θ_{gim}. A monopulse system can be gimbaled in order to scan a broader area than the beamwidths of the antennas. In order to optimally cover the

entire 360 degrees field of regard (FOR), our system used two monopulse radar configurations with one at each end of the aircraft. This configuration is shown in Figure 1 (a) and (b).

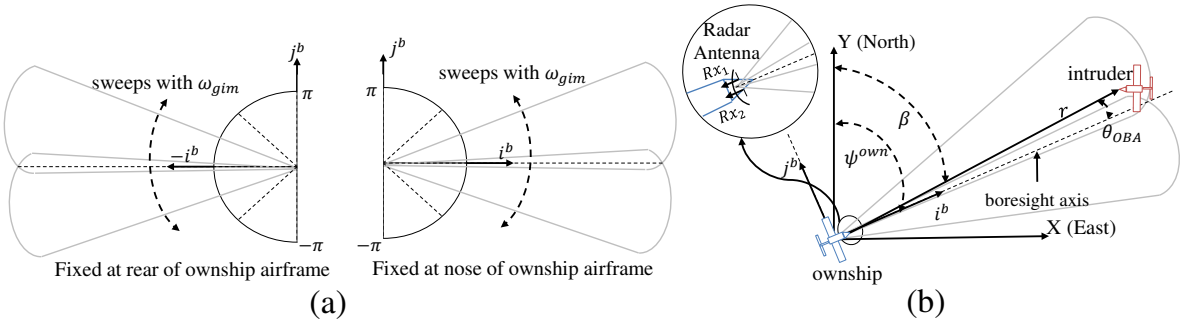

Fig. 1 (a) Two radar units on-board the ownship, each is sweeping back and forth to cover 180 **degrees. (b) We assumed that the boresight axes (antenna system axes) are aligned with the ownship body axes. The (i^b-j^b) coordinates represent the body frame of the ownship and (X-Y) is the global coordinate system.**

With radar, there is generally a trade-off between tracking and searching capabilities. The nature of the problem being solved in this paper requires a search mode radar that will scan the entire FOR. However, when monopulse tracking methods are applied, an angular accuracy much finer than the antenna beamwidth can be obtained [23]. In order to integrate monopulse into the radar search mechanism, the radar system scans across the entire FOR at a series of discrete look angles and averages several radar returns at each angle. When a target is detected at one of the look angles, the monopulse method is applied to fine tune the initial detection angle, θ_{gim}. The angular correction, or off-boresight angle (θ_{OBA}), is determined by comparing the sum and the difference of the two receive antenna amplitudes, Rx_1 and Rx_2, and is given by

$$\theta_{\text{OBA}} \approx \frac{\theta_{3dB}}{k_m} \frac{\Delta}{\sum}, \tag{1}$$

where θ_{3dB} is the 3 dB beam width of the antenna, $\Delta = Rx_1 - Rx_2$, $\sum = Rx_1 + Rx_2$, and k_m is a linearity factor with a value between 1 and 2 [23]. The bearing to the intruder is given by

$$\beta = \theta_{gim} + \theta_{\text{OBA}} + \psi^{own} \tag{2}$$

where ψ^{own} is the heading of the ownship.

The monopulse method drastically improves the initial angle estimate provided by the gimbal

Table 1 Simulated FMCW Radar Parameters

Parameter	Value	Parameter	Value
Transmitted Power (P^{rad})	1 W	Center Frequency	10.25 GHz
Chirp Period (T_c)	1 ms	Chirp Bandwidth	50 MHz
TX Antenna Gain (G^t)	14.83 dB	TX Antenna Beamwidth	40 degrees Azimuth
RX Antenna Gain (G^r)	17.57 dB	RX Antenna Beamwidth	20 degrees Azimuth
Gimbal rotation rate	360 degree/s	TX and RX Beamwidth	40 degrees Elevation
System Noise Figure (F)	6.02 dB	FFT Noise Bandwidth B_{noise}	1 kHz

angle in a way that is computationally inexpensive and cheap to implement in hardware. The angular estimation can be improved further by switching the radar to track mode and pointing the gimbal at the predicted angle and iterating through successive monopulse approximations and gimbal adjustments until the off-boresight angle is zero and the boresight angle of the gimbal is equal to the angle of the target. However, since this problem necessitates a search mode radar, the gimbal continues rotating and the slight angular error introduced by using a single monopulse iteration is accounted for in the Kallman Filter used to track the radar returns. The power received by each antenna as a function of angle and range is given by

$$P_{rec}(\theta, r) = \frac{P^{rad} G^t(\theta) G^r(\theta) \mathrm{RCS} \lambda^2}{(4\pi)^3 r^4}, \tag{3}$$

where P^{rad} is the power radiated, $G^t(\theta)$ and $G^r(\theta)$ are the gains of the transmitter and receiver respectively, RCS is the radar cross section of the target, λ is the wavelength and r is the range to the target. The angle θ used in Eq. (3) is the off-boresight angle from each antenna individually and should not be confused with the off-boresight angle of the combined monopulse system. The signal-to-noise ratio (SNR) for our model is given by

$$SNR = \frac{P_{rec}}{P_{noise,thermal} + P_{noise,system} + P_{noise,clutter}} \approx \frac{P_{rec}}{P_{noise,thermal} F}. \tag{4}$$

Our model uses the standard approximation where system, thermal, and clutter noise sources are lumped into a single value that multiplies the thermal noise with a noise figure F for the system that approximates the contribution from system noise and clutter. We use the standard equation

for thermal receiver noise given by

$$P_{noise,thermal} = k_B T_0 B_{noise}, \tag{5}$$

where k_B is the Boltzmann constant, T_0 is standard temperature 290 K, and B_{noise} is the bandwidth of a Fast Fourier Transform (FFT) bin over which the noise is observed. To produce the simulated radar returns we create a time-domain signal with amplitude given by Eq. (3) as a function of the true range and bearing to the intruder with respect to the gimbal pointing angle. Noise is added as given by Eq. (4) and the resulting signal is passed through an FFT to produce realistic radar range compressed data that undergoes monopulse processing to generate a bearing estimate. Using Eq. (4), the radar parameters listed in Tabel 1 result in approximately 10 dB of SNR for 0.1 m^2 RCS at a range of 800 m.

III. States Estimation

The problem of estimating the time evolution of the position, velocity and acceleration of an intruder from sequential sensor measurements has been previously addressed in the literature [24, 25]. The measurements provided by the radar sensor i.e. range, bearing (azimuth), elevation, and possibly the range rate are polar in nature; while the intruder dynamics are best expressed in rectangular coordinates. Since practical estimators, such as least squares and Kalman filters, operate under assumptions of linearity, there is a problem in directly applying the Kalman filter to measurements that are nonlinear in the state. The approximation residuals which result from linearization can accumulate and, unless preventive measures are taken, may cause the estimator to diverge from the intruder's true state [26, 27]. On the other hand, the EKF is one of the most popular approaches to handle nonlinear measurements. It performs implicit coordinate transformation by linearizing the measurement model through a Taylor series expansion. However, it was shown that transforming a zero-mean measurement error from polar to rectangular coordinates generates a bias error [28]. As a consequence, debiased filtering techniques were proposed and validity limits on the applicability of the EKF were derived [29, 30]. In this paper, we adopted an alternative approach in which the state and measurement equations are formulated in the so-called modified polar coordinates (MPC). The resulting EKF has been shown to be stable and an asymptotically

unbiased estimator [19, 20]. Consider the scenario shown in Figure 1 (b), where both the intruder and the ownship are flying at the same fixed altitude. Let the state vector $\mathbf{x}$ represent the Cartesian coordinates of the relative position and velocity between intruder and ownship at time t where

$$\mathbf{x} = \begin{bmatrix} x_1(t) \\ x_2(t) \\ x_3(t) \\ x_4(t) \end{bmatrix} \triangleq \begin{bmatrix} p_x(t) \\ p_y(t) \\ v_x(t) \\ v_y(t) \end{bmatrix} \triangleq \begin{bmatrix} p_x^{int}(t) - p_x^{own}(t) \\ p_y^{int}(t) - p_y^{own}(t) \\ v_x^{int}(t) - v_x^{own}(t) \\ v_y^{int}(t) - v_y^{own}(t) \end{bmatrix}. \tag{6}$$

Let $\mathbf{y}$ denote the modified polar coordinate state vector, given as

$$\mathbf{y} \triangleq [\dot{\beta}(t), \dot{r}(t)/r(t), \beta(t), 1/r(t)]^\top, \tag{7}$$

where $r(t) = \sqrt{p_x^2(t) + p_y^2(t)}$ and $\beta(t) = \text{atan2}(p_x(t), p_y(t))$ are the range and bearing to the intruder provided by the radar sensor at time t, respectively. It is shown in Ref. [19, 20], that the time evolution of state vector $\mathbf{y}$ is given by

$$\dot{\mathbf{y}} = \begin{bmatrix} \dot{y}_1(t) \\ \dot{y}_2(t) \\ \dot{y}_3(t) \\ \dot{y}_4(t) \end{bmatrix} = \begin{bmatrix} -2y_1(t)y_2(t) + y_4(t)[\dot{x}_1(t)\cos(y_3(t)) - \dot{x}_2(t)\sin(y_3(t))] \\ y_1^2(t) - y_2^2(t) + y_4(t)[\dot{x}_1(t)\sin(y_3(t)) + \dot{x}_2(t)\cos(y_3(t))] \\ y_1(t) \\ -y_2(t)y_4(t) \end{bmatrix}. \tag{8}$$

Since in modified polar coordinates the state propagation model is nonlinear and the measurement update model is linear, the continuous-discrete EKF is a good choice for this application [31]. The continuous-discrete EKF assumes that the process evolution and measurement equations have the form

$$\dot{\mathbf{y}} = f(\mathbf{y}(t)) + \xi, \tag{9}$$

$$\mathbf{z}[n] = C\mathbf{y}[n] + \eta[n] \tag{10}$$

where $\mathbf{z}[n] = \mathbf{z}(t_n)$ is the n^{th} sample of $\mathbf{z}$ and $C = [0\ 0\ 1\ 0; 0\ 0\ 0\ 1]$. The signals ξ and η are the process and measurement noise, respectively and are zero-mean Guassian random variables with known covariance matrices. While the process noise covariance is a tuning parameter, the covariance matrix of the measurement are determined by the noise properties of the radar [24, 32, 33]. A one-to-one nonlinear transformation which maps the MPC state vector $\mathbf{y}(t)$ into its rectangular counterpart

$\mathbf{x}(t)$ is given by

$$\mathbf{x}(t) = f_x[\mathbf{y}(t)] = \frac{1}{y_4}\begin{bmatrix} \sin(y_3) \\ \cos(y_3) \\ y_2\sin(y_3) + y_1\cos(y_3) \\ y_2\cos(y_3) - y_1\sin(y_3) \end{bmatrix}. \tag{11}$$

Using Eq. (6), and given that the states of ownship are known, the position, speed and heading of the intruder can be estimated as

$$p_x^{int}(t) = x_3(t) + p_x^{own}(t), \tag{12}$$

$$p_y^{int}(t) = x_2(t) + p_y^{own}(t), \tag{13}$$

$$v^{int}(t) = \sqrt{\Big(x_3(t) + v_x^{own}(t)\Big)^2 + \Big(x_4(t) + v_y^{own}(t)\Big)^2}, \tag{14}$$

$$\psi^{int}(t) = \text{atan2}\Big(x_3(t) + v_x^{own}(t), x_4(t) + v_y^{own}(t)\Big). \tag{15}$$

To show the performance of the sensor and estimator, we simulate a simple case scenario similar to

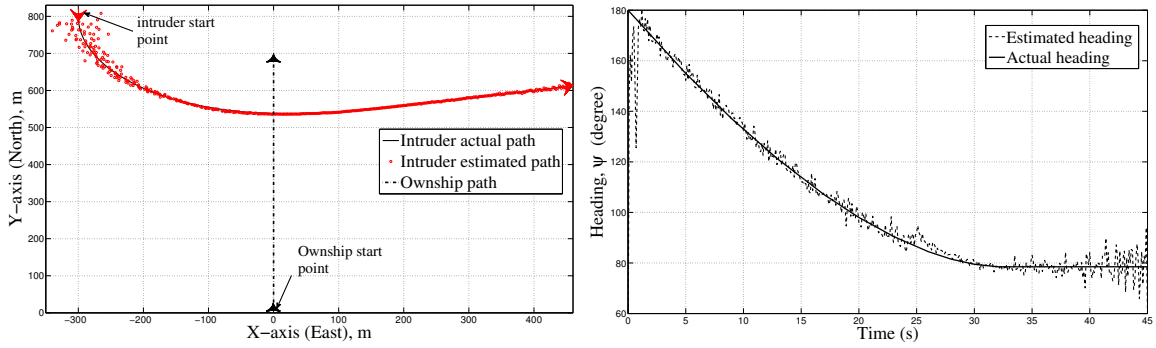

(a) (b)

Fig. 2 Actual and estimated track (a) and heading (b) of the intruder.

the planner geometry shown in Figure 1(b) The ownship starts at position (0,0) with initial heading of 0 degrees and moving with constant speed of 15 m/s. The intruder starts at position (-300, 800) with 180 degrees with respect to the Y-axis (North) and moving at speed of 20 m/s. The path of the ownship, the actual and estimated path of the intruder are shown in Figure 2 (a). The noise variances of the simulated range and bearing measurements are $\sigma_r = 0.87$ m and $\sigma_\beta = 2.72$ degrees considered for RCS=1 m^2. The aircraft dynamics are simulated using a simplified model that captures the flight characteristics of UAS. The actual and estimated heading, velocity components,

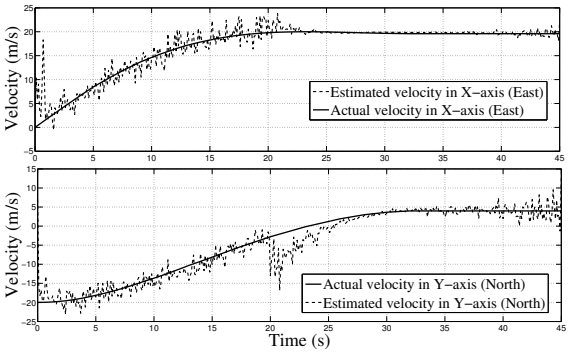

(a) Actual and estimated velocity components of the intruder.

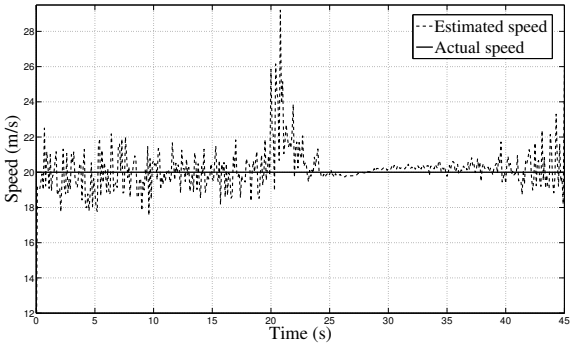

(b) Actual and estimated speed of the intruder.

Fig. 3 Actual and estimated velocity components (a) and speed (b) of the intruder.

and speed states of the intruder are shown in Figure 2(b), Figure 3(a) and (b), respectively. For further analysis on initialization, design and performance of MPC EKF, we refer the interested reader to Ref. [19, 20].

IV. Encounter Maneuver Model

Generally, not every aircraft that is observed by the detection system presents a collision threat. The ownship should only maneuver to avoid aircraft when a collision threat exists. Unnecessary course changes limit flight efficiency and may confuse other airspace users. Therefore, the collision detection determines whether an approaching intruder is on a collision course or not. For the ease of exposition, we will restrict the attention to the 2D case since the generalization to 3D is straight forward. Let $\mathbf{r}^{\text{int}} = (x, y)^\top \in \mathbb{R}^2$ denotes the position of the intruder. The motion of the intruder is described by the Dubins kinematic model of the aircraft flying in the 2D plane with constant speed and subject to an upper bound on the curvature of its path [34]. The kinematics motion model is given by

$$\dot{x} = v \cos\psi(t), \tag{16}$$

$$\dot{y} = v \sin\psi(t), \tag{17}$$

$$\dot{\psi} = u, \tag{18}$$

where v is the intruder speed and $u \in \mathcal{S}_{\dot{\psi}}$ where $\mathcal{S}_{\dot{\psi}} \triangleq \left\{ \left| \dot{\psi} \right| \leq \dot{\psi}_c \right\}$ is the set of possible turn rate inputs. The system of differential equations (16)-(18) can be represented as

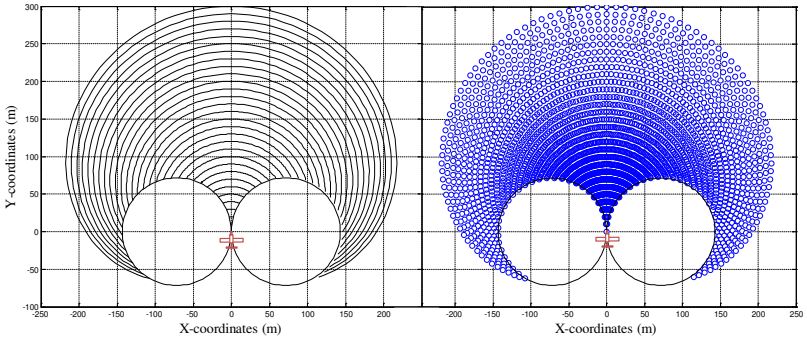

Fig. 4 (a) The level curves of reachable sets $\mathcal{R}_{rd}(\tau, t_0, \mathbf{w}_0)$ generated using Eqs. (16)-(18) from $\mathbf{w}_0 = (0,0,0)^\top$ for $u = [-8, 8]$ degree/s, and $v = 10$ m/s over $\tau = [0, 30]$ seconds. (b) The discrete-time approximation, $\mathcal{R}(\ell, t_0, \mathbf{w}_0)$ generated with $\delta_u = \frac{16}{m}$ degree/s, $m = 100$, and $T_s = 1$ second for $\ell = 1, 2, \cdots, 30$.

$$\dot{\mathbf{w}} = f(\mathbf{w}, u), \ |u| \leq \dot{\psi}_c \tag{19}$$

where $\mathbf{w} \triangleq (x, y, \psi)^\top$ is the system states and u is the system input. We introduce the notation of the reachable set to describe the region in the space that is accessible at time τ by the aircraft from the initial state $\mathbf{w}_0$ at time t_0.

Definition 1. Let $\hat{w}(\tau, t_0, w_0, u(\cdot))$ be the solution of the system $\dot{w} = f(\mathbf{w}, u)$ at $\tau \geq t_0$ from the initial condition $\mathbf{w}_0$ and with input $u(\cdot)$ where $u(\tau) \in \mathcal{S}_{\dot{\psi}}$. The definition of the reachable set at time τ, given the initial state $\mathbf{w}_0$ at the initial time t_0 is

$$\mathcal{R}(\tau, t_0, \mathbf{w}_0) \triangleq \{\xi \in \mathbb{R}^{\mathbf{n}} | \exists \text{ input } u(\cdot) \text{ such that } \hat{w}(\tau, t_0, w_0, u(\cdot)) = \xi\}.$$

The reachable sets $R(\tau, t_0, w_0)$ for increasing values of $\tau \geq t_0$ are shown in Figure 4(a). To obtain a discrete-time approximation, we quantize the input as $\mathcal{S}_{u_d} = \{-\dot{\psi}_c, -\dot{\psi}_c + \delta_u, \cdots, -\dot{\psi}_c + m\delta_u, \dot{\psi}_c\}$ where $\delta_u = \frac{2\dot{\psi}_c}{m}$ and $m \in \mathbb{Z}_+$. Applying a zero order hold to the equations of motion (16)-(18) with sample size T_s we get

$$x_{k+1} = x_k + T_s v \, \text{sinc}(\frac{T_s u_k}{2\pi}) \cos(\psi_k + \frac{T_s u_k}{2}), \tag{20}$$

$$y_{k+1} = y_k + T_s v \, \text{sinc}(\frac{T_s u_k}{2\pi}) \sin(\psi_k + \frac{T_s u_k}{2}), \tag{21}$$

$$\psi_{k+1} = \psi_k + T_s u_k. \tag{22}$$

The reachable set for the discrete dynamics with quantized input is defined as follows.

Definition 2. Let $\hat{w}_d(\ell, t_0, w_0, u_d(\cdot))$ be the solution of the system $w_{k+1} = f_d(w_k, u_k)$ at time $t = t_0 + \ell T_s$, where $\ell = 1, 2, \cdots, L$ is the discrete look-ahead index, starting from the initial condition $\mathbf{w}_0$ and with input $u_d(\cdot)$ where $u_d(t_0 + kT_s) \in \mathcal{S}_{u_d}$. The definition of the reachable set at time ℓ, given the initial state $\mathbf{w}_0$ at the initial time t_0 is

$$\mathcal{R}(\ell, t_0, \mathbf{w}_0) \triangleq \{\xi \in \mathbb{R}^{\mathbf{n}} | \ \exists \text{ input } u_d(\cdot) \text{ such that } \hat{w}_d(\ell, t_0, w_0, u_d(\cdot)) = \xi\}.$$

Note that the size of the discretized input set $\mathcal{S}_{u_d}$ is $m+1$, which implies that the cardinality of the discrete-time reachable set $\mathcal{R}_d(\ell, t_0, \mathbf{w}_0)$ is $(m+1)^\ell$ states. To manage the exponential growth of the size of $\mathcal{R}_d(\ell, t_0, \mathbf{w}_0)$ observe that aircraft tend to maneuver slowly, and that the most likely future trajectory, at least over the near term, is to hold the current speed and turn rate. Therefore, we will limit the reachable set to those states that can be reached with constant input trajectories $u_d(\ell_1) = u_d(\ell_2)$ for all $\ell_1, \ell_2 = 1, \ldots, L$. We denote this set as $\mathcal{R}_{rd}(\ell, t_0, \mathbf{w}_0)$ and note that its cardinality is $(m+1)$. Figure 4(b) shows the reduced discrete reachable set with a fixed number of configurations along each level curve.

Having determined the region of accessibility of the intruder over a look-ahead window, the question becomes: What is the probability that the intruder will reach a specific configuration point within the reachability region? To answer this question we use the transition probabilities contained in the MIT LL UEM. The MIT LL UEM is a high fidelity probabilistic airspace encounter model based on actual radar data collected from more than 120 radar sites across the United States and is statistically representative of the behavior of aircraft maneuvering in close proximity to each other. The MIT LL UEM is based on the use of Bayesian networks to represent relationships between the airspace class A, altitude layer L, speed v, acceleration $\dot{v}$, turn rate $\dot{\psi}$, and climb rate $\dot{h}$. The airspace class A is divided into four values (class B, C, D and O) where O represent other airspace class such as the uncontrollable airspace class G. Altitude layer is also divided into four layers, 500-1200, $1200-3000$, 3000-5000 and 5000-18000 feet above the ground level. The continuous variables, such as the turn rate $\dot{\psi}$, is quantized into seven bins symmetric about zero, [-8, -6], [-6, -4.5], [-4.5, -1.5], [-1.5, 1.5], [1.5, 4.5], [4.5, 6] and [6, 8] degree/s from which a specific value is then sampled uniformly [12, 35]. Consider a collision encounter where the ownship and the intruder are flying in a specific airspace class and altitude layer. Let $\hat{\mathbf{r}}(t)$, $\hat{v}(t)$, and $\hat{\dot{\psi}}(t)$ be the ownship's estimates of

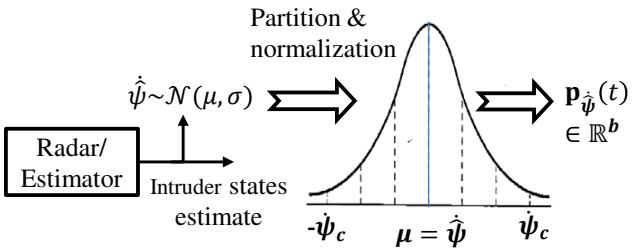

Fig. 5 The state probability vector, $\mathbf{p}_{\dot{\hat{\psi}}}(t)$ can be obtained through partitioning and normalizing $p_{\dot{\hat{\psi}}}(\dot{\hat{\psi}})$ over the discrete bins of $\dot{\psi}$

the current intruder's position, speed and turn rate, respectively. Then these estimates determine where to look in the transition probability tables of the MIT LL UEM. We can extract from these tables the probabilities of each possible candidate of $\dot{\psi}(t+T_s)$ jointly conditioned on A, L, $\hat{v}(t)$ and $\dot{\hat{\psi}}(t)$. These transition probabilities can be represented by a one-time step transition probability matrix $M_{\text{trans}} \in \mathbb{R}^{b\times b}$, where b is the number of the turn rate discrete bins defined in the MIT LL UEM. Assuming that the estimated turn rate, $\dot{\hat{\psi}}(t)$ is normally distributed with $\dot{\hat{\psi}} \sim \mathcal{N}(\mu, \sigma)$ and the associated probability density function (pdf) is $p_{\dot{\hat{\psi}}}(\dot{\hat{\psi}})$. Suppose that the pdf of the turn rate estimate can be represented by a discrete state probability vector $\mathbf{p}_{\dot{\hat{\psi}}}(t) \in \mathbb{R}^{1\times b}$. As shown in Figure 5, the state probability vector $\mathbf{p}_{\dot{\hat{\psi}}}(t)$ at the current time t can be obtained by partitioning and normalizing $p_{\dot{\hat{\psi}}}(\dot{\hat{\psi}})$ over the turn rate range $\dot{\psi} \in [-\dot{\psi}_c, \dot{\psi}_c]$. Now, we would like to propagate $p_{\dot{\hat{\psi}}}(\dot{\hat{\psi}})$ over the time horizon $[t, t+\ell T_s]$ using the one-step transition probability M_{trans}. However, the MIT LL UEM transition distribution table projects the transition probabilities one time step into future while our approach requires the knowledge of the probability distribution over the time horizon. A possible solution is to employ the concept of the n-steps transition probability matrix of a discrete Markov random process. The probability distribution of a discrete Markov process after n$\geq$ 1 transitions is completely determined by the one-step transition probability matrix and the initial state probability vector. Similarly, the probability distribution of $\dot{\hat{\psi}}$ or the state probability vector $\mathbf{p}_{\dot{\hat{\psi}}}(t)$ propagated ℓ time steps into the future can be given by

$$\mathbf{p}_{\dot{\hat{\psi}}}(t+\ell T_s) = \mathbf{p}_{\dot{\hat{\psi}}}(t) M_{\text{trans}}^{\ell}. \tag{23}$$

Let $\mathbf{P}_{\text{tran}} \in \mathbb{R}^{b \times L}$ be the vector of all the state probability vectors $\mathbf{p}_{\dot{\psi}}(\tau_d)$, defined as

$$\mathbf{P}_{\text{tran}} \triangleq [\mathbf{p}_{\dot{\psi}}^{\top}(t+T_s), \mathbf{p}_{\dot{\psi}}^{\top}(t+2T_s), \ldots, \mathbf{p}_{\dot{\psi}}^{\top}(t+LT_s)]^{\top}. \tag{24}$$

The b quantization intervals for $\dot{\psi}$ define b wedges in the reachability set. As shown in Figure 6(a) we will denote these wedges by $W_i, i = 1, \ldots, b$. The current model does not account for the uncertainty associated with the intruder's position, velocity and heading estimates. However, we have assumed that the reachable sets are determined based on the current estimate of position, velocity and heading estimates of the intruder provided by the radar/tracker which represent the mean of their respective distribution.

V. Collision Risk Estimation

The purpose of computing the collision risk is to have an alert threshold value above which the collision avoidance system is triggered to initiate an evasive maneuver to avoid an imminent collision with the detected intruding aircraft. There are a number of approaches to evaluate the future collision risk of an encounter situation. Most of these approaches can either be classified as geometric or probabilistic, where each approach has different techniques to deal with errors. In the geometric approach, the collision risk is described based on the geometric relationship between aircraft. Aircraft trajectory predictions are based on linear projections of current aircraft states such that the uncertainty of the predicted trajectory is translated into areas around the predicted trajectory referred as to safe zones. Linear projections can be computationally efficient and, prediction errors are negligible over short time horizons [36, 37] or assumed known when flight plans are communicated [38]. On the other hand, the probabilistic methods estimate the probability of collision based on a probabilistic model of future intruder dynamics. This event probability is then compared to a certain threshold above which the aircraft is deemed to be in collision. These probabilities can be estimated using approximate analytical solution [5], numerical approximation [39, 40], Monte Carlo methods [13, 41, 42]. The expected utility is another approach used to develop a risk alerting system that accounts for future changes in alerts and the responses to them [43]. In general, the probabilistic approaches are computationally intensive but suffer less from false alarms than geometric approaches. Our work is similar to the threshold-based probabilistic methods. However,

rather than making simplifying assumptions in order to derive an analytical solution or performing a computationally expensive sampling to account for all possible states, our approach presents a tradeoff that accounts for all likely intruder trajectories with a computational scheme that can be handled by limited resources available on board small UAS.

Let $\mathbf{r}^{\text{own}}(t)$ be the position of the ownship and let $\hat{\mathbf{r}}^{\text{int}}(t)$ be the estimated position of the intruder at the current time t. The protected zone of the ownship is a virtual region centered on the ownship, usually represented by a circular disk with radius d_{safe}, defined as

$$\mathcal{B}_{d_{\text{safe}}}(\mathbf{r}^{\text{own}}(t)) = \left\{\mathbf{d} \in \mathbb{R}^2 : \|\mathbf{r}^{\text{own}}(t) - \mathbf{d}\| \leq d_{\text{safe}}\right\}.$$

The encounter situation is said to generate a collision if the intruder enters $\mathcal{B}_{d_{\text{safe}}}$. The collision risk is the largest probability of a collision event over the look ahead window $\tau \in [t, t + \ell T_s]$. The probability of collision at step $\ell = 1, \ldots, L$ is computed as

$$P_{\text{col}}(\ell, t) = \bigcup_{w \in R_d(\ell, t, \hat{w}(t))} \mathcal{I}\left[w \in \mathcal{B}_{d_{\text{safe}}}(\mathbf{r}^{\text{own}}(t + \ell T_s))\right] P\left(\left\{\mathbf{r}^{\text{int}}(t + \ell T_s) = w\right\}\right), \tag{25}$$

where $\mathcal{I}[\cdot]$ is the indicator function, and $P\left(\{\mathbf{r}^{\text{int}}(t + \ell T_s) = w\}\right)$ is the probability of the event that the actual future state of the intruder at time $t + \ell T_s$ will be w. In this paper, the future predicted position of the ownship is given given by

$$\mathbf{r}^{\text{own}}(t + \ell T_s) = \mathbf{r}^{\text{own}}(t) + \ell T_s v^{\text{own}}(t)(\cos\psi^{\text{own}}(t), \sin\psi^{\text{own}}(t))^\top,$$

where $\mathbf{r}^{\text{own}}(t)$, $v^{\text{own}}(t)$, and $\psi^{\text{own}}(t)$ are the current position, speed, and course of the ownship.

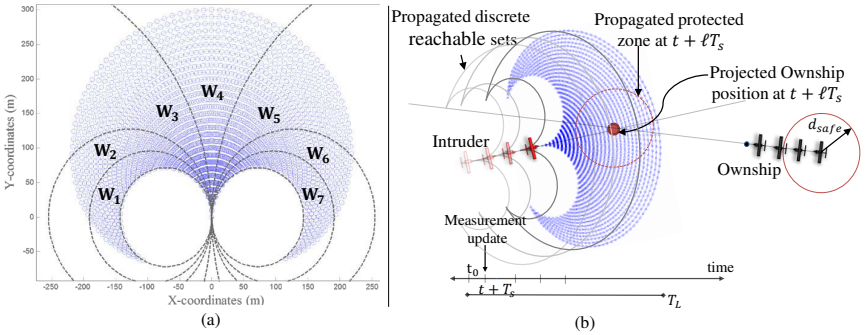

Fig. 6 The b quantization intervals for $\dot{\psi}$ define b wedges in the reachability set. In this example $b = 7$ (a). The collision risk is continuously evaluated while the locus of reachable sets is updated after every new measurement (b).

As indicated in Figure 6, the probability of collision at step ℓ given in Eq. (25) is the number of states belonging to the intersection between the reachable set $\mathcal{R}_d(\ell, t, \mathbf{r}^{\text{int}}(t))$ and the safe zone $\mathcal{B}_{d_{\text{safe}}}(\mathbf{r}^{\text{own}}(t + \ell T_s))$ relative to the total number of states in the relative wedges, weighted by the corresponding transition probabilities in the ℓ^{th} column of $\mathbf{P}_{\text{tran}}$. If we use the notation $|\mathcal{A}|$ to denote the cardinality of the discrete set $\mathcal{A}$, then we have

$$P_{\text{col}}(\ell, t) = \sum_{i=1}^{b} \frac{|\mathcal{R}_{rd}(\ell, t, \mathbf{r}^{\text{int}}(t)) \bigcap \mathcal{B}_{d_{\text{safe}}}(\mathbf{r}^{own}(t + \ell T_s)) \bigcap W_i|}{|\mathcal{R}_{rd}(\ell, t, \mathbf{r}^{\text{int}}(t)) \bigcap W_i|} \mathbf{P}_{\text{tran}}(\ell, i). \tag{26}$$

To account for the fact that there are many paths to each location, and that the input trajectory for the intruder may not have been constant, we modify Equation (26) to include several fronts on reachable set as

$$P_{\text{col}}(\ell, t) = \frac{1}{2\mathcal{L} + 1} \sum_{m=\ell-\mathcal{L}}^{\ell+\mathcal{L}} \sum_{i=1}^{b} \frac{|\mathcal{R}_{rd}(m, t, \mathbf{r}^{\text{int}}(t)) \bigcap \mathcal{B}_{d_{\text{safe}}}(\mathbf{r}^{own}(t + \ell T_s)) \bigcap W_i|}{|\mathcal{R}_{rd}(m, t, \mathbf{r}^{\text{int}}(t)) \bigcap W_i|} \mathbf{P}_{\text{tran}}(m, i), \tag{27}$$

where $\mathcal{L}$ is the size of the window of level curves inside the safe zone at time step ℓ. To maximize the safety of the system, the maximum collision risk estimate is evaluated over the look ahead window $\ell \in [1, L]$ as

$$P_{\text{col}}(t) = \max_{\ell \in [1, L]} P_{\text{col}}(\ell, t). \tag{28}$$

Generally, the collision risk involves extracting some measure of how the current encounter situation is critical compared to a threshold $\mathcal{C}_D$. If the threshold is exceeded i.e. $P_{\text{col}}(t) \geq \mathcal{C}_D$, then the collision detection logic issues an alert to declare that the detected intruder is on a collision course. As shown in Figure 6(b), the collision risk is evaluated regularly, that is, after every new measurement the state estimates of the intruder and the locus of reachable configurations is updated with respect to the new estimated location and orientation of the intruder. In addition, the transition probability assignment is updated over the course of the collision encounter depending on the estimated air class, altitude level, speed, acceleration, and heading rate variations of the intruder. The collision risk is continuously evaluated after every measurement update using Eq. (28).

VI. Simulation Results and Assessment

To provide a performance measure of the proposed collision detection approach, the performance measure is quantified in terms of the signal detection metrics of probability of correct detection P_{cd}

and probability of false alarm P_{fa} [7, 44]. A Monte Carlo simulation is used to generate the system operating characteristic (SOC) curve that can be used to illustrate the tradeoff between correct detections and false alarms. The SOC curves can be also used to pick the decision threshold that yields the optimal correct detections and false alarms. If $\mathcal{N}$ is the number of performed simulations, among which there are $\mathcal{E}$ true collision encounters for a specific decision threshold $\mathcal{C}_D$, and the proposed collision detection algorithm detects $\mathcal{M}$ collision encounters, among which $\tilde{\mathcal{E}}$ encounters are the true collision events, then the correct detection rate P_{cd} and false alarm rate P_{fa} are given by

$$P_{cd} = \frac{\tilde{\mathcal{E}}}{\mathcal{E}}, \qquad P_{fa} = \frac{\mathcal{M} - \tilde{\mathcal{E}}}{\mathcal{N} - \mathcal{E}}.$$

By varying $\mathcal{C}_D$ for different sizes of intruder aircraft, we obtain P_{cd} and P_{fa} as a function of $\mathcal{C}_D$. Plotting P_{cd} versus P_{fa} as $\mathcal{C}_D$ varies gives us the SOC curve for targets of varying sizes. To validate

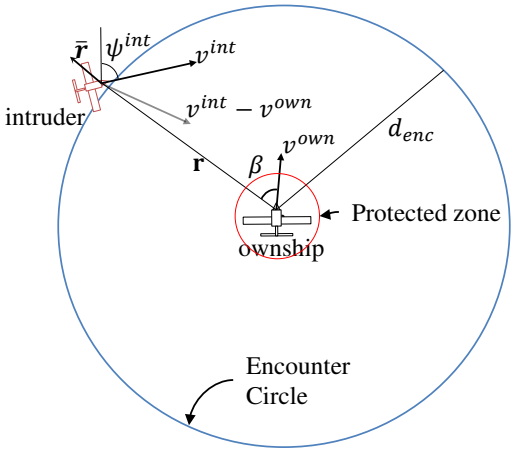

Fig. 7 The encounter geometry used for Monte Carlo simulations.

the performance of the radar sensor model, the estimation scheme, and the collision detection algorithm, we create a simulation environment with 4 degree-of-freedom aircraft models for both the ownship and intruder. We assume that both the ownship and intruder are flying at the same altitude. To generate realistic encounter scenarios that are representative of what is observed in the national airspace, we sample flight trajectories from the MIT LL UEM. However, the following constraints are considered when sampling the intruder trajectories from the MIT LL UEM. The encounter scenarios are assumed to take place in class G airspace flying within an altitude layer of

500-1200 ft. The initial airspeed of the intruder varies over (0, 65] m/s based on the type of the intruder used in the simulation. In addition, the control variables $\dot{v}$ and $\dot{\psi}$ vary from -2 to 2 m/s^2 and -8 to 8 degree/s, respectively while the climb rate $\dot{h}$ is set to 0 m/s. To construct the encounter geometry we follow an approach suggested by M.J. Kochenderfer et al. [12]. We assume a virtual encounter circle centered on the ownship. The radius of the encounter circle is set to $d_{enc} = 800$ m. The ownship is initialized at the center of the encounter circle $\boldsymbol{p}^{\text{own}}(t_0) = (0, 0)$ and follows a straight line path. However, at each Monte Carlo run the intruder is randomly initialized on the perimeter of the encounter circle. The bearing angle of the intruder relative to the ownship is drawn from a uniform distribution over $[0, 2\pi]$ and the heading of the intruder is randomly drawn from a uniform distribution over $[0, 2\pi]$ while the ownship heading is set to 0 degree. The simulated encounters are similar to the planner geometry shown in Figure 7. The radar parameters used in simulation are listed in Table 1. The procedure of the Monte Carlo simulations consists of the following steps.

1. The trajectories of both the ownship and intruder are generated over a 45 s time horizon where the sample time is set to 0.1 s.

2. At each run, the intruder is initialized on the perimeter of the encounter circle, with a random heading that ensures that the intruder is penetrating the encounter region at the first time instant.

3. For each Monte Carlo simulation trial, execute the collision detection algorithm. A collision threat is declared as soon as the collision risk measure $P_{\text{col}}(t)$ exceeds the threshold $\mathcal{C}_D$. The definition of collision threat detection accounts for the fact that a collision may be detected before it is too late to take an action. In these simulation, a collision threat alert is considered valid if it is declared at least 10 s before the collision would actually occur.

4. We compute the probability of false alarm and the probability of correct detection for each collision threshold value and plot the system operating characteristic curve, P_{cd} versus P_{fa}. A thousand Monte Carlo simulation runs are conducted for each collision threshold value.

We repeated the Monte Carlo simulation procedure for small, medium, and large sized intruder aircraft. We define a large intruder aircraft as having a wingspan greater than 15 ft, similar to a

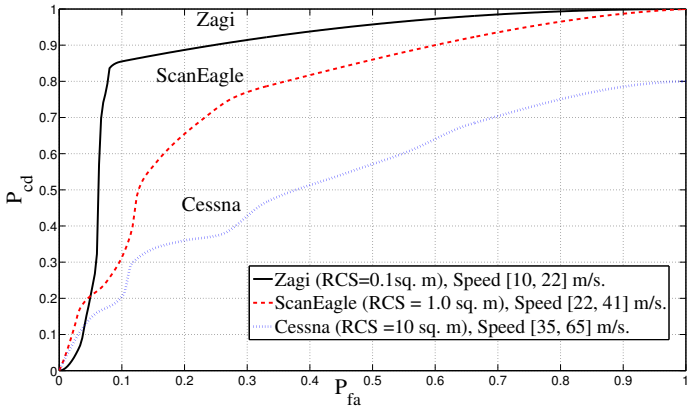

Fig. 8 The P_{cd} and P_{fa} versus different threshold values examined for different intruder types.

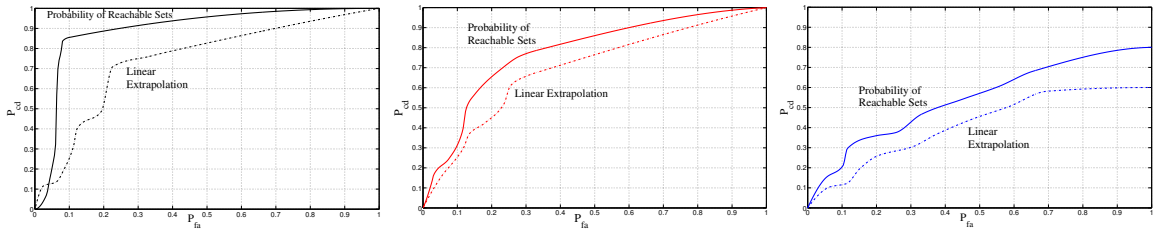

(a) Zagi size intruder. (b) ScanEagle size intruder. (c) Cessna size intruder.

Fig. 9 SOC curves for our approach (solid line) and simple linear extrapolation (dashed line) for three different intruder in terms of size and speed variations.

Cessna aircraft. We define a medium size intruder as having a 10-15 ft wingspan similar to that of a ScanEagle, and a small intruder UAS as having a wingspan less than 10 ft, similar to a Zagi. The intruder aircraft are assumed to have RCS sizes of 0.1, 1, and 10 m^2 for small, medium, and large aircraft, respectively [45]. The authors note that while these RCS values are approximate, the performance of the system over such a wide range 20 dB of RCS fluctuation demonstrates its efficacy. Commercial aircraft will generally have RCS values much larger than 10 m^2 and small UAS will have RCS close to 0.1 m^2 [45]. To be consistent we use identical path trajectory profiles sampled from MIT LL UEM for the different sized intruder aircraft. The SOC curves for the three different intruder aircraft obtained by Monte Carlo simulation are shown in Figure 8. Note that an ideal collision detection algorithm would operate at the point $P_{fa} = 0$ and $P_{cd} = 1$, i.e. all collision threats are detected and there are no false alarms. However, the closer the SOC curve is to the point $(0, 1)$ the better the performance will be. Although, smaller size intruders like the Zagi have

a lower RCS value that causes the radar/tracker to produce poor estimates, the low speeds of this aircraft allow an adequate amount of time for the tracker to converge, thus helping the collision detection algorithm to perform better.

Finally, we compare the performance achieved by our proposed approach with a simplified scheme where the future position of the intruder is projected by propagating the current position along a straight in the direction of the current heading. This comparison is conducted by repeating Monte Carlo procedure applying similar geometric and flight path profiles for the ownship and the intruder, and using the same parameters for the radar sensor and estimator. The SOC results shown in Figure 9 indicate that our algorithm outperforms the linear extrapolation approach. However, since the comparison results show that the difference in performance is not huge, the computationally simple approach of linear extrapolation might be efficiently used along with the probabilistic approach in a multi-tiered collision detection system.

VII. Conclusion

We have introduced in this paper a probabilistic based collision detection and risk estimation approach that computationally feasible for small UAS. The proposed collision approach has the advantage that the locus of states within the reachable sets with respect to the detected intruder are only computed once, which makes it attractive and feasible for real-time SAA on board small UAS. The computational burden is expected to be much less than existing algorithms that require running Monte Carlo approximations in near real time or performing an extensive sampling from the probability distribution of intruder estimated states or probabilistic encounter models. The average simulation time required to execute one cycle of our collision detection code is 0.00355 seconds. This small run time motivates the application of this algorithm to multiple intruder scenarios. We introduced a realistic radar model which could be built and implemented on-board small UAS. Although several standards have suggested that the necessary field of regard for a sense and avoid system should be 220 degrees or 240 degrees in the azimuthal plane, our simulations and analysis have extended this to a full 360 degrees to account for overtaking scenarios.

This work could be extended in a number of ways. Extending the work to 3D and non-level

flight is an important step toward flight implementation. An additional future task is to account for the uncertainty in position and velocity of the intruder and to assess acceptable uncertainty bounds. Another task is to pair the collision detection logic with a suitable avoidance algorithm. In addition, investigating other types of sensors would also enhance this work.

Acknowledgments

This research was conducted in the Center for Unmanned Aircraft Systems (C-UAS) with support from the National Science Foundation I/UCRC program grant number #IIP-1171036 and C-UAS Industry Advisory Board members (see http://c-uas.byu.edu for current membership.)

References

[1] Dalamagkidis, K., Valavanis, K. P., and Piegl, L. A., *On Integrating Unmanned Aircraft Systems into the National Airspace System*, Vol. 52, Springer Science+Business Media B.V., 2nd ed., 2012.

[2] Kuchar, J. K. and Yang, L. C., "A review of conflict detection and resolution modeling methods," *IEEE Transactions on Intelligent Transportation Systems*, Vol. 1, No. 4, 2000, pp. 179–189.

[3] Albaker, B. M. and Rahim, N. A., "Unmanned Aircraft Collision Detection and Resolution: Concept and Survey," *2010 5th IEEE Conference on Industrial Electronics and Applications*, pp. 248–253.

[4] Angelov, P., *Sense and Avoid in UAS: Research and applications*, John Wiley & Sons, Ltd., 2012.

[5] Paielli, R. A. and Erzberger, H., "Conflict probability estimation for free flight," *AIAA Guidance, Control, and Dynamics*, Vol. 20, No. 3, 1997, pp. 588–596.

[6] Hu, J., Lygeros, J., Prandini, M., and Sastry, S., "Aircraft Conflict Prediction and Resolution using Brownian Motion," in "Proceedings of the 38th Conference on Decision & Control," Phoenix, December, 1999.

[7] Adaska, J. W., "Computing Risk For Unmanned Aircraft Self Separation With Maneuvering Intruders," in "Digital Avionics Systems Conference," IEEE, 2012.

[8] Weibel, R. E., Edwards, M. W. M., and Fernandes, C. S., "Establishing a Risk-Based Separation Standard for Unmanned Aircraft Self Separation," in "Proceedings of the ninth USA/Europe Air Traffic Management Research & Development Seminar," Berlin, Germany: Eurocontrol/FAA, June, 2011.

[9] Temizer, S., Kochenderfer, M. J., Kaelbling, L. P., Lozano-Pérez, T., and Kuchar, J. K., "Collision Avoidance for Unmanned Aircraft using Markov Decision Processes," in "Proceedings of the AIAA Guidance, Navigation and Control Conference and Exhibit," , 2010.

[10] Geyer, C., Singh, S., and Chamberlain, L., "Avoiding Collisions Between Aircraft: State of the Art and Requirements for UAVs operating in Civilian Airspace," Tech. rep., 2008.

[11] Chen, W.-Z., Kay, J., and Raska, V. M., "Autonomous Sense and Avoid (SAA) for Unmanned Air Systems (UAS)," in "NATO Research and Technology Organisation (RTO), RTO-SCI-202," , 2009.

[12] Kochenderfer, M. J., Kuchar, J. K., Espindle, L. P., and Griffith, J. D., "Uncorrelated Encounter Model of the National Airspace System Version 1.0," Tech. Rep. November, Lincoln Laboratory-Masschusetts Institute of Technology, Lexington, 2008.

[13] Jackson, J. and Boskovic, J., "Application of Airspace Encounter Model for Prediction of Intruder Dynamics," in "AIAA Modeling and Simulation Technologies Conference," American Institute of Aeronautics and Astronautics, Guidance, Navigation, and Control and Co-located Conferences, 2012.

[14] Enright John J., Ketan Savla, Emilio Frazzoli, F. B., "Stochastic and Dynamic Routing Problems for Multiple Uninhabited Aerial Vehicles," *Journal of Guidance, Control, and Dynamics*, Vol. 32, No. 4, 2009, pp. 1152–1166.

[15] Mitchell, I. M., Bayen, A. M., and Tomlin, C. J., "A Time-Dependent Hamilton-Jacobi Formulation of Reachable Sets for Continuous Dynamic Games," *IEEE Transactions on Automatic Control*, Vol. 50, No. 7, 2005, pp. 947–957.

[16] Frew, E. and Sengupta, R., "Obstacle avoidance with sensor uncertainty for small unmanned aircraft," in "43rd IEEE Conference on Decision and Control," Vol. 1, 2004, pp. 614–619.

[17] Cockayne, E. J. and Hall, G. W. C., "Plane Motion of a Particle Subject to Curvature Constraints," *SIAM*, Vol. 13, No. 1, 1975, pp. 197–220.

[18] Sahawneh, Laith R. and Beard, R. W., "A probabilistic Framework for Unmanned Aircraft Systems Collision Detection and Risk Estimation," in "53rd IEEE Conference on Decision and Control," IEEE, Los Angeles, California, December 15-17, 2014.

[19] Farina, A., "Target Tracking with Bearings Only Measurements," *Signal Processing*, Vol. 78, No. October 1998, 1999, pp. 61–78.

[20] Aidala, V. J. and Hammel, S. E., "Utilization of Modified Polar Coordinates for Bearings-Only Tracking," *IEEE Transactions on Automatic Control*, Vol. 28, 1982, pp. 283–294.

[21] Contarino, M. and Scire Consultants, L., "All Weather Sense and Avoid System for UASs," Tech. rep., Report to the Office of Naval Research, 2009.

[22] Edrich, M., "Ultra-Lightweight Synthetic Aperture Radar Based on a 35 GHz FMCW Sensor Concept and Online Raw Data Transmission," *IEEE Proceedings-Radar, Sonar and Navigation*, Vol. 153, No. 2, 2006, pp. 129–134.

[23] Richards, M. A., Scheer, J., and Holm, W. A., *Principles of Modern Radar: Basic Principles*, SciTech Publishing, Inc., 2010.

[24] Yaakov Bar-Shalom X. Rong Li, T. K., *Estimation with Applications to Tracking and Navigation*, John Wiley & Sons, Ltd, 2001.

[25] Subhash Challa, Mark R. Morelande, Darko Mušicki, R. J. E., *Fundamentals of Object Tracking*, Cambridge University Press, New York, 2011.

[26] Miller, K. S. and Leskiw, D. M., "Nonlinear Estimation With Radar Observations," *IEEE Transactions on Aerospace and Electronic Systems, AES*, Vol. AES-18, No. 2, 1982, pp. 192–200.

[27] Bishop, A. N., Pathirana, P. N., and Savkin, A. V., "Target Tracking with Range and Bearing Measurements via Robust Linear Filtering," *2007 3rd International Conference on Intelligent Sensors, Sensor Networks and Information*, , No. 1, 2007, pp. 131–135.

[28] Schlosser Markus S. and Kroschel Kristian, "Limits in Tracking with Extended Kalman Filters," *IEEE Transactions on Aerospace and Electronic Systems*, Vol. 40, No. 4, 2004, pp. 1351–1359.

[29] Z. Zhao, X. L. and Jilkov., V., "Best Linear Unbiased Filtering with Nonlinear Measurements for Target Tracking." *IEEE Transactions on Aerospace and Electronic Systems*, Vol. 40, No. 4, 2004, pp. 1324–1336.

[30] Lerro D. and Bar-Shalom Y, "Tracking with Debiased Consistent Converted Measurements Versus EKF," *IEEE Transactions on Aerospace and Electronic Systems, AES*, Vol. 29, No. 3, 1993, pp. 1015–1022.

[31] Beard, R. and McLain, T., *Small Unmanned Aircraft: Theory and Practice*, Princeton University Press, 1st ed., 2012.

[32] Grewal, Mohinder, S. and Andrews, A. P., *Kalman Filtering: Theory and Practice Using MATLAB*, John Wiley & Sons, Ltd, New York, 2008.

[33] Zarchan, Paul and Musoff, H., *Fundamentals of Kalman Filtering: A Practical Approach*, AIAA, New York, 2008.

[34] Dubins, L. E., "On Curves of Minimal Length with a Constriant on Average Curvature and with Prescribed Initial and Terminal Positions and Tangents," *American Journal of Mathematics*, Vol. 79, No. 3, 1957, pp. 497–516.

[35] Kochenderfer Mykel J., Espindle Leo P., Kuchar James K., Griffith, J. D., "A Comprehensive Aircraft Encounter Model of the National Airspace System," *Lincoln Laboratory Journal*, Vol. 17, 2008, pp. 41–53.

[36] Geser, A. and Muñoz, C., "A Geometric Approach to Strategic Conflict Detection And Resolution

[ATC],” in “Proceedings of the 21st IEEE Digital Avionics Systems Conference,” Vol. 1, 2002, pp. 6B1–1–6B1–11.

[37] Chiang, Y.-J., Klosowski, J. T., Lee, C., and Mitchell, J. S. B., “Geometric Algorithms for Conflict Detection/Resolution in Air Traffic Management,” in “Proceedings of the 36th IEEE Conference on Decision and Control,” Vol. 2, 1997, pp. 1835–1840.

[38] Muñoz, C., Narkawicz, A., and Chamberlain, J., “A TCAS-II Resolution Advisory Algorithm,” in “Proceedings of the AIAA Guidance, Navigation, and Control Conference,” Boston, Massachusetts, AIAA-2013-4622, 2013.

[39] van Daalen, C. and Jones, T., “Fast conflict detection using probability flow,” *Automatica*, Vol. 45, 2009, pp. 1903–1909.

[40] Lauderdale, T. A., “Probabilistic Conflict Detection for Robust Detection and Resolution,” in “12th AIAA Aviation Technology, Integration and Operation (ATIO) Conference and 14th AIAA/ISSM,” Indianapolis, IN., 2012.

[41] Lindsten, F., Nordlund, P.-J., and Gustafsson, F., “Conflict Detection Metrics for Aircraft Sense and Avoid Systems,” in “Proceedings of the 7th IFAC Symposium on Fault Detection, Supervision and Safety of Technical Processes (SafeProcess),” Spain, 2009.

[42] Lee, Y., Yang, J. H., Kuchar, J., and Feron, E., “A Real-Time Monte Carlo Implementation for Computing Probability of Conflict,” in “Proceedings of the AIAA Guidance, Navigation and Control Conference and Exhibit,” Vol. 178, 2004, pp. 1835–1840.

[43] Chryssanthacopoulos, J. P. and Kochenderfer, M. J., “Hazard Alerting Based on Probabilistic Models,” *Guidance, Control, and Dynamics*, Vol. 35, No. 2, 2012, pp. 442–450.

[44] Kuchar, J. K., “Methodology for Alerting-System Performance Evaluation,” *Guidance, Control, and Dynamics*, Vol. 19, No. 2, 1996, pp. 438–444.

[45] Morchin, W., *Radar Engineer’s Sourcebook*, Artech House, pp. 110–118, 1993.